Available online at www.sciencedirect.com
ScienceDirect
Journal of Power Sources 170 (2007) 28–37
JOURNAL OF POWER SOURCES
www.elsevier.com/locate/jpowsour

Kinetics and mechanism for the oxygen reduction reaction on polycrystalline cobalt–palladium electrocatalysts in acid media

William E. Mustain *, Jai Prakash

Department of Chemical and Environmental Engineering, Center for Electrochemical Science and Engineering, Illinois Institute of Technology, Chicago, IL 60616, United States

Received 20 February 2007; received in revised form 28 March 2007; accepted 3 April 2007
Available online 10 April 2007

Abstract

Cobalt–palladium ($CoPd_x$) bimetallic electrocatalysts of various compositions were prepared and their physical and electrochemical properties were examined. The nominal composition of the polycrystalline electrocatalysts was estimated by energy dispersive X-ray analysis (EDX) and the lattice parameters were evaluated using X-ray diffraction (XRD). Electrocatalytic activity of the $CoPd_x$ electrodes for the oxygen reduction reaction was compared using cyclic voltammograms obtained in oxygen saturated, 0.5 M H_2SO_4. $CoPd_3$ was identified as having the highest activity, showing peak currents comparable to a polycrystalline Pt electrode under identical experimental conditions. The rotating disk electrode technique was used to collect kinetic data for the oxygen reduction on $CoPd_3$ and the activity of the binary electrocatalysts was evaluated. Kinetic and mechanistic aspects of the oxygen reduction reaction on $CoPd_3$ are discussed and specific ways in which the surface structures may be involved are proposed.

Keywords: Oxygen reduction; Palladium; Catalyst; Fuel cell; Pt free; Mechanism

1. Introduction

The sluggish kinetics of molecular oxygen on various electrocatalytic surfaces is a problem of great importance [1–4] and the oxygen reduction reaction (ORR) has become one of the most extensively studied electrochemical reactions. In the past several years, considerable progress has been made in understanding the ORR on Pt and Pt-based bimetallic alloy electrocatalysts. Several investigations have been carried out to determine the role of alloying on the electrocatalytic activity [5–16] and much of this experimental work has indicated that the catalytic activity of Pt-based bimetallic clusters towards the ORR in acid media is at least as good as that of pure platinum.

Various explanations have been put forward to describe the effect of alloying on the electrocatalytic activity. It has been suggested by Mukerjee and coworkers [7,8] that the bimetallic surface may exist with a platinum skin and an alloy underlayer where the electronic properties of the surface Pt atoms are modified. This was also proposed by Toda et al. where the enhancement of the oxygen reduction currents was explained by a shift in the d-band electronic density, Pt coordination number and tuning of the Pt–Pt interatomic distance [17]. Alloying may also inhibit the formation of the adsorbed hydroxyl species, Pt–OH, which has been found on all the low index platinum surfaces [18].

On the other hand, Balbuena et al. suggested that enhancement of the catalytic activity is due to the presence of the secondary metal on the catalyst surface, where alloys of Pt with cobalt and chromium are optimal for the dissociative adsorption of O_2 [19]. Balbuena also proposed that further enhancement in the performance of Pt alloys with limited amounts of another transition metal like Co or Cr, may be explained by both tuning the interatomic distance as well as providing an increase in the electron density [20] at the catalytic sites. These results are in agreement with the work of both Mukerjee [7,8] and Stamenkovic [5] who have shown that Pt–Co and Pt–Cr alloys have the highest activity, at least twice that of pure Pt.

The generalized mechanism for the ORR in acid media [21,22] is presented in Fig. 1. Bulk oxygen approaches the surface by diffusive mass transport where two parallel reaction

* Corresponding author. Tel.: +1 312 567 3639; fax: +1 312 567 8874.
E-mail address: mustwil@iit.edu (W.E. Mustain).

0378-7753/$ – see front matter © 2007 Elsevier B.V. All rights reserved.
doi:10.1016/j.jpowsour.2007.04.005

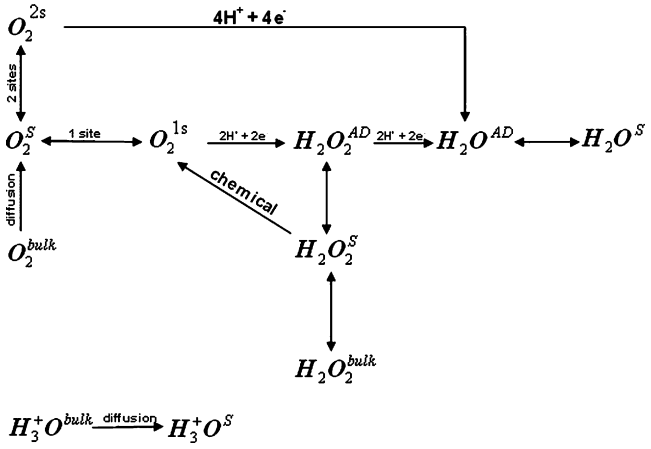

Fig. 1. Mechanism for the electrochemical reduction of molecular oxygen in acid media. The reduction proceeds through two pathways, a dual site, direct four-electron reduction to water and a single site peroxide route where either two or four electron and proton transfers occur.

pathways occur and the dominant reaction pathway is determined by the type of molecular chemisorption. Depending on the interaction of O_2 with the catalyst surface, the oxygen reduction will either proceed via a two-site adsorption leading to the direct four-electron reduction of oxygen to water or end-on adsorption for the peroxide route, which may rearrange to yield a dual-bond, single site adsorption. An illustration of the adsorbed oxygen reduction precursors is shown in Fig. 2. For each adsorption type, protonation may either precede or follow adsorption, depending on the degree of proton solvation and the distance between the oxygen molecule and the surface [23,24]. The resulting product is either an adsorbed MOMOH species for the direct pathway, Eq. (1), or MOOH species for the peroxide pathway, Eq. (2).

$$2M + O_2 + e^- + H^+ \rightarrow MOMOH_{ads} \quad (1)$$

$$M + O_2 + e^- + H^+ \rightarrow MOOH_{ads} \quad (2)$$

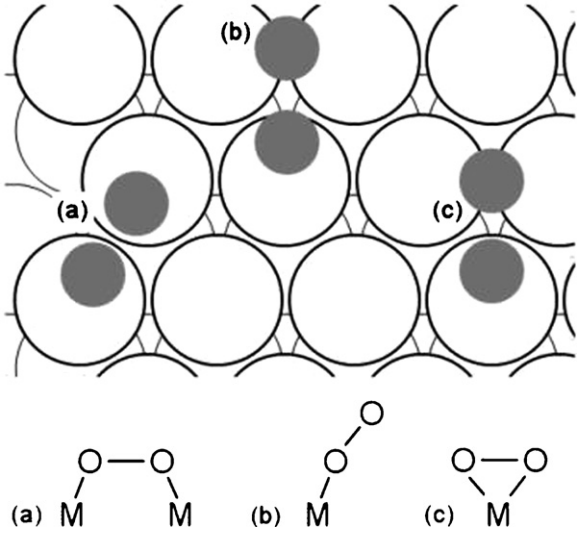

Fig. 2. Schematic diagram for molecular oxygen adsorption sites on the (1 1 1) face of face centered cubic transition metal electrocatalysts. The adsorption sites are labeled corresponding to the Yeager (a), Pauling (b) and Griffiths (c) models.

If the mechanism proceeds via the direct route, the first electron transfer is followed by the dissociation of the oxygen bond.

$$MOMOH_{ads} \rightarrow MO_{ads} + MOH_{ads} \quad (3)$$

If we consider a bimetallic electrocatalyst where the second metal participates in the adsorption, Eqs. (1) and (3) can be rewritten to incorporate both metallic sites M_1 and M_2.

$$M_1 + M_2 + O_2 + e^- + H^+ \rightarrow M_1OM_2OH_{ads} \quad (4)$$

$$M_1OM_2OH_{ads} \rightarrow M_1O_{ads} + M_2OH_{ads} \quad (5)$$

For the peroxide route, the second electron and proton transfer steps may follow two processes. They may either lead to the formation of water and an adsorbed oxygen atom or a hydrogen peroxide-like intermediate depending on which O the proton attacks [23], which is shown in Eqs. (6) and (7), respectively.

$$MOOH_{ads} + M + H^+ + e^- \rightarrow MO_{ads} + MOH_{2ads} \quad (6)$$

$$MOOH_{ads} + M + H^+ + e^- \rightarrow MOHOH_{ads} \quad (7)$$

The peroxide intermediate from Eq. (7) is then either desorbed to complete the stunted two-electron mechanism or further decomposed. The possible 3rd and 4th electron and proton transfer steps complete the four electron reduction leading to water formation.

This advanced understanding of the reaction mechanism, coupled with the systematic decomposition of the crucial steps of the ORR in acid media using both experimental and theoretical data, have led at least two groups to develop criterion for the development of highly active catalysts for the ORR. In a recent communication, Zhang et al. [25] used the density functional theory method to calculate activation energies for the oxygen bond dissociation as well as the hydrogenation of atomic oxygen. They reported that electrocatalysts that fell in the vicinity of the intersection of the two activation energy trend lines had the highest activity for the ORR. On the other hand, Fernandez et al. reported a simple thermodynamic model for the design of bimetallic electrocatalysts for the ORR [26]. This work helps to explain the remarkable activity reported by a few groups for a family of cobalt–palladium electrocatalysts [27–30], though the complete ORR mechanism on these materials remains uncharacterized.

In this paper, the electrocatalytic activity of polycrystalline $CoPd_x$ electrocatalysts for the ORR are studied in an oxygen saturated, aqueous, 0.5 M H_2SO_4 electrolyte. The composition of the alloy surfaces was characterized by SEM/EDX and lattice parameters were determined by XRD. It is demonstrated that the $CoPd_3$ composition shows the highest catalytic activity for the ORR, comparable to polycrystalline platinum under identical experimental conditions. The RDE technique is used to collect kinetic data for the ORR on polycrystalline $CoPd_3$. The RDE data is decomposed to reveal kinetic and mechanistic aspects of the oxygen reduction reaction on $CoPd_3$ and specific ways in which the surface structures may be involved is proposed.

2. Experimental

The polycrystalline $CoPd_x$ electrodes used in this study were prepared by two methods. First, the flag-type electrodes used in the cyclic voltammetry experiments were prepared by electrodeposition in a dual ligand, aqueous plating bath [31–33]. Two independent solutions were prepared. The first system employed an ammonium salt, in this case ammonium sulfate, which forms an activated ligand complex with palladium ions in solution, which are added by dissolving $PdSO_4$. The solubility of the salt was controlled by lowering the pH of the solution by adding sulfuric acid. Then, a two-fold excess of ammonium sulfate was added to the solvated palladium salt. In the second solution, glutaric acid is introduced to a cobalt-ion solution to form a carboxylic conjugate base-cobalt complex. First, $CoSO_4{\cdot}xH_2O$ is dissolved in water, followed by an excess of the glutaric acid. Both solutions were stirred for at least 24 h. Ammonium hydroxide was added to each solution until the pH was between 8 and 9. The solutions were then combined to give plating baths of desired composition, where the composition of the electrodeposit is given by Eq. (8).

$$\frac{N_{Co}}{N_{Pd}} = K(T)\frac{C_{Co}}{C_{Pd}} \tag{8}$$

where the plating constant, $K(T)$, was determined as 0.31 at 35 °C. The solution was bubbled with argon for 2 h. Polycrystalline gold electrodes are then immersed in solution and deposition of the bimetallic electrocatalyst was conducted at −1.49 V (NHE) for 900 s. The electrodes were removed from solution, rinsed with deionized water and polished with 0.05 μm alumina particles to a mirror finish.

Second, unsupported $CoPd_3$ nanoparticles, for use in the rotating disk electrode experiments, was synthesized using the capping polymer method outlined by Miyazaki et al. [34] where poly *N*-isopropylacrylamide (Sigma–Aldrich) was used as the capping polymer. 1.0 g of poly *N*-isopropylacrylamide was solvated in 100 mL of 18 MΩ Millipore water. Initially, 2.0 g $Pd(NO_3)_2$ (Sigma–Aldrich) was added to the polymer mixture. H_2 gas was bubbled for 1 h and the container was sealed overnight to allow for complete reduction of the Pd ions. A stoichiometric amount of $Co(NO_3)_2{\cdot}6H_2O$ was then added to the Pd/polymer mixture with 5 g L^{-1} sodium bicarbonate and allowed to stir for 30 min before bubbling with H_2 gas for an additional hour to reduce the cobalt ions. The slurry was then filtered, rinsed and dried under vacuum and the resulting powder was heated to 550 °C for 2 h to both remove the supporting polymer and allow the two metals to incorporate.

Kinetic measurements were made with the $CoPd_3$ nanoparticles using the rotating disk electrode (RDE) technique. The graphite disk electrode assembly (Pine Instrument Company) was modified so that the disk was recessed slightly below (∼100 μm) the outer plane of the Teflon mounting to create a very small cavity over the disk electrode. A polytetrafluoroethylene (60 wt% PTFE, Sigma–Aldrich) suspension was diluted with water and ultrasonically agitated with the $CoPd_3$ nanoparticles. The resulting mixture was 5 wt% in PTFE solids. This semi-moist paste was kneaded with a spatula and then applied to the disk, spread evenly and allowed to dry overnight in inert atmosphere. The resulting electrode was polished to a mirror finish with 0.05 μm alumina powder.

Prior to each experiment, the $CoPd_x$ working electrodes were washed with both fresh electrolyte and 18 MΩ Millipore water and electrochemically cycled at 10 mV s^{-1} twenty times between −0.2 and 1.2 V versus the normal hydrogen electrode (NHE) to ensure a clean, active surface. The electrodes were inserted into a three compartment glass cell with a Luggin capillary and several polarization experiments were completed at the same scanrate. The cyclic voltammograms were performed at room temperature, 22 °C, while the RDE experiments were conducted 25 °C, which was maintained by a circulating water bath. The electrolyte solutions were prepared with Millipore water and ultrapure sulfuric acid (Sigma–Aldrich). The electrolyte was bubbled with Ar for 2 h before saturation with oxygen. The polarization curves were measured with an Autolab PGSTAT30 potentiostat and the electrode rotation speed was controlled by an AFMSRX analytical rotator (Pine Instrument Company).

3. Results and discussion

3.1. Physical characterization of $CoPd_x$ electrocatalysts

The approximate elemental composition of the prepared electrocatalysts was determined by energy dispersive X-ray spectroscopy (EDX) on a scanning electron microscope (SEM) with an integrated EDX apparatus. Light elements like carbon, sulfur and oxygen were neglected in the analysis. The primary electron energy for the analysis was 20 keV. At this energy, the analysis depth is larger than the deposition thickness, approximately 1 μm, evidenced by the fact that the signals corresponding to the gold substrate in the polycrystalline electrodeposits were detected.

A cross-sectional SEM micrograph for the electrodeposited $CoPd_3$ electrode is shown in Fig. 3. As shown in the micrograph, the surface roughness of the electrodeposit is dependent

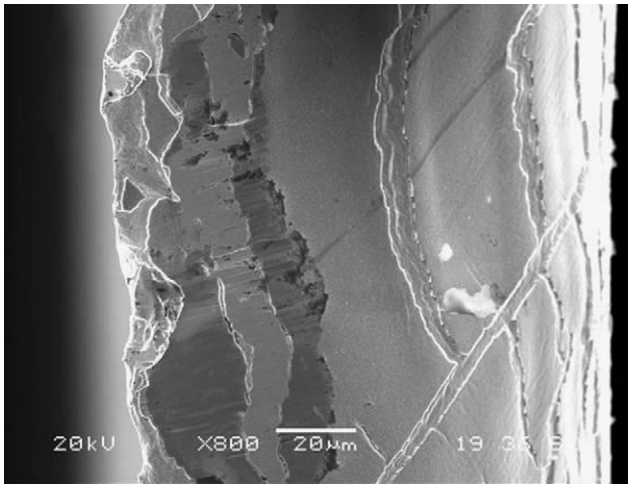

Fig. 3. Cross-section scanning electron micrograph of the $CoPd_3$ catalyst electrodeposited on a polycrystalline gold electrode in a dual ligand bath, 35 °C.

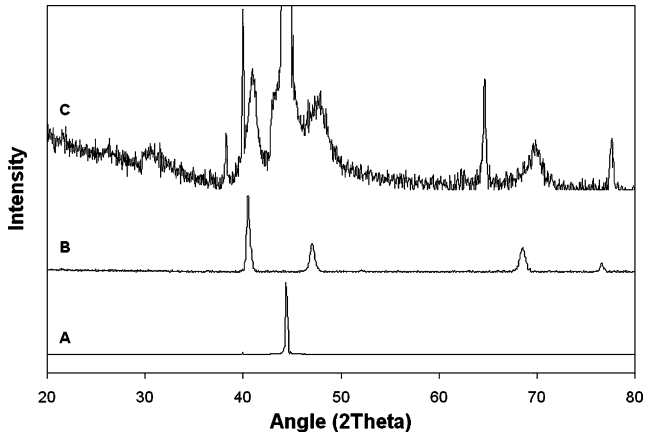

Fig. 4. X-ray diffraction pattern for the polycrystalline deposition substrate (A), polycrystalline Pd (B) and electrodeposited $CoPd_2$ (C).

on the orientation of the working electrode in solution with respect to the counter electrode during the deposition process. The electrode plane facing the counter electrode exhibits much less roughness than the rear, where the mobility of ions between the working and counter electrodes encounter a much higher resistance. It should be noted that the surface has been slightly bent to allow for the surface features of the smooth face to be observed more clearly. Also, it is shown that during the deposition process, stress cracks have appeared on the surface of the deposit. This is likely due to structural stresses during electrodeposition caused by both hydrogen uptake by palladium atoms as well as mild H_2 evolution at the low electrode potential. Further tuning of the plating bath may be needed in order to lessen the effect, including the addition of a brightener or wetting agent, though it does not appear to significantly alter either the surface area or the electrochemical performance.

The crystal structure of the electrochemically deposited $CoPd_x$ catalysts was examined by XRD. Fig. 4 shows a typical XRD pattern for a cobalt–palladium bimetallic electrocatalyst ($CoPd_2$) as well as XRD patterns for polycrystalline Au and polycrystalline Pd. Each of the Co–Pd electrocatalysts show a similar single-phase fcc XRD pattern to that of the polycrystalline Pd sample with incorporated peaks belonging to the Au substrate. This indicates that the crystal structure of the prepared catalysts was a single fcc phase regardless of the atomic composition, including the pure Pd case.

According to the binary phase diagram, cobalt and palladium form solid solutions at any atomic ratio at high temperature. Because the catalysts were prepared by deposition in solution at low temperature and exhibit a single-phase XRD, it is likely that the electrocatalysts are a metastable solid solution phase, since a three-phase (Pd-rich, CoPd and $CoPd_3$) equilibrium is thermodynamically favored at lower temperatures. However, in the temperature range of interest in this investigation, phase segregation would not occur since diffusion of the Co and Pd atoms is very limited at such low temperatures.

The (1 1 1) diffraction peaks of the various $CoPd_x$ electrocatalysts were used to determine the lattice parameters. On Pd and its alloys, the (1 1 1) peak is observed around $2\Theta = 40$–42°. The lattice parameters were calculated using Eq. (9).

Table 1
Peak angle and lattice parameters for several $CoPd_x$ catalysts using X-ray diffraction

$CoPd_x$ composition (% Pd)	Peak angle (2Θ)	Lattice parameter (Å)
Pd (100)	40.5	3.85
$CoPd_4$ (80)	40.75	3.83
$CoPd_3$ (75)	40.90	3.82
C_6Pd_2 (67)	40.96	3.81
CoPd (50)	40.98	3.81

$$\sin^2\Theta = \frac{\lambda^2}{4\delta^2}(h^2 + k^2 + q^2) \quad (9)$$

where λ is the Cu Kα radiation wavelength, 1.54 Å, δ the lattice parameter and h, k and q are the lattice index parameters. The results are summarized in Table 1. It was found that the peaks of the (1 1 1) reflection shifted to higher angles with increasing Co content, indicating a lattice contraction arising from the substitution of the smaller Co atoms for Pd. The lattice parameter and Co content show an approximately linear relationship over the whole Co–Pd system. This result supports the fact that the prepared $CoPd_x$ electrocatalysts are a solid solution phase as described above. It was also observed that the width of the (1 1 1) diffraction peak was consistent for all electrocatalysts, indicating that the crystallite size was independent of Co content; however, the peak width of all of the electrocatalysts was larger than the polycrystalline Pd sample, indicating that the crystallinity of the $CoPd_x$ catalysts may be reduced when compared to Pd.

3.2. Effect of composition on the ORR activity of cobalt–palladium bimetallic catalysts

Cyclic voltammograms for electrochemically deposited $CoPd_2$ and $CoPd_3$ working electrodes in argon purged, oxygen saturated 0.5 M H_2SO_4 at 25 °C are compared in Fig. 5. Since each of the electrodes was polished to a mirror finish with 0.05 μm alumina powder in order to reduce the surface roughness, the current density was obtained by normalizing the

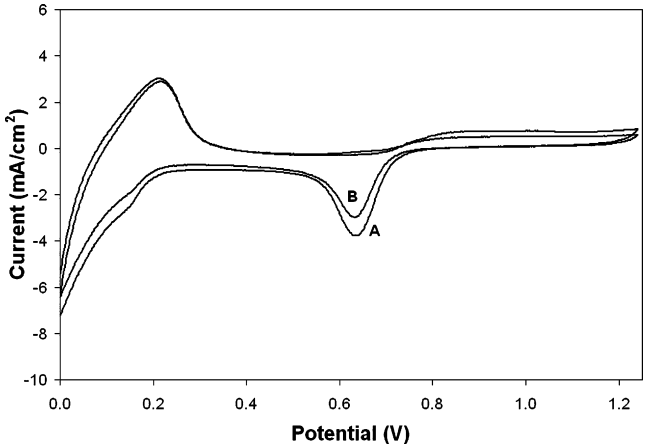

Fig. 5. Cyclic voltammogram for $CoPd_3$ (A) and $CoPd_2$ (B) flag-type electrodes in oxygen saturated 0.5 M H_2SO_4 at 22 °C, 10 mV s^{-1}.

observed current to the geometric electrode area. Both of these voltammograms are representative of $CoPd_x$ voltammograms over a wide range of compositions (17–50 at.% cobalt) where all of the prepared Pd electrocatalysts exhibit a large hydrogen peak below 0.4 V versus NHE. It is clear from Fig. 5 that the areas under this peak, as well as the magnitude of the currents in the double layer region, are comparable for all of the electrocatalysts. This equivalence implies that both the surface roughness and the electrochemically active area of the deposited electrode materials are independent of electrode composition. However, as evidenced by the curves in Fig. 5, differences are observed in the area under both the anodic oxidation and cathodic reduction scans. The differences in activity suggest that despite the similarity in the structure of the electrochemical interface, some of the electrocatalysts have sites that are more energetically favorable for the oxidation and reduction reactions. Also, in Fig. 5, it is shown that the cathodic peak potential attributed to the ORR, located slightly negative of 0.65 V, is independent of electrocatalyst composition. Using an expression for the peak position of an irreversible reaction, E_p, the constant peak position over the range of catalyst composition seems to indicate that the kinetic rate constant, k_i, is the same for all of the electrocatalysts [35].

$$E_p = E^{0'} - \frac{RT}{\alpha F}\left[0.780 + \ln\left(\frac{D_o^{1/2}}{k_i}\right) + \ln\left(\frac{\alpha F \upsilon}{RT}\right)^{1/2}\right] \quad (10)$$

where k_i is the kinetic rate constant, α the transfer coefficient and υ is the scanrate.

Therefore, if both the rate constant and the electrochemically active areas of the polished surfaces are comparable, this seems to support a surface-site mechanism where the reduction reaction occurs at specific sites and the difference in activity is due to a change in the number of active sites for the ORR rather than a change in the kinetic rate constant.

In order to examine the effect of Co content on the ORR activity on polycrystalline electrodeposited $CoPd_x$ electrocatalysts, peak currents for the cathodic voltammetric sweep were compared for several compositions between 17 and 50 at.% cobalt. The results are summarized in Fig. 6 where the peak current is plotted as a function of electrocatalyst composition. The highest

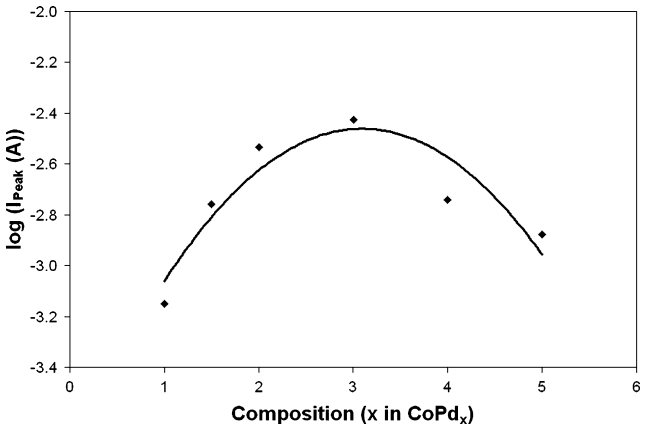

Fig. 6. Peak cathodic voltammogram current for the ORR on $CoPd_x$ bimetallic electrocatalysts in oxygen saturated, 0.5 M H_2SO_4 at 22 °C, 10 mV s^{-1}.

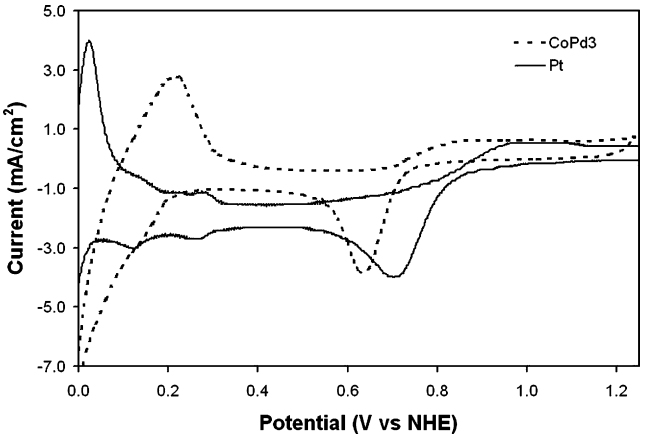

Fig. 7. Comparison cyclic voltammograms for polycrystalline platinum and electrochemically deposited $CoPd_3$ electrodes in 0.5 M H_2SO_4 electrolyte, 22 °C.

electrocatalytic activity was observed for an atomic composition of 25% Co. This chemical composition is similar to previous reports in which the highest activity was found on Pd alloys with various secondary transition metal composition of 70–80 at.% Pd [26–30]. Also, since the voltammetric data in Fig. 5 indicated a site mechanism is active for the ORR, it may be concluded that $CoPd_3$ is the most likely composition for the electrochemically active site for the oxygen reduction reaction on this family of bimetallic catalysts.

Comparison cyclic voltammograms for the electrochemically deposited $CoPd_3$ and polished polycrystalline platinum foil (Sigma–Aldrich) electrodes in argon-purged, oxygen saturated 0.5 M H_2SO_4 at 22 °C are shown in Fig. 7. The platinum voltammogram is typical of those reported in previous studies [1,29,36–38]. Characteristic platinum peaks are observed just prior to 0.25 V for hydrogen underpotential deposition, H_{upd}, and hydrogen oxidation during the cathodic and anodic scans, respectively. Typical behavior is also observed at higher potentials, where the onset of platinum metal oxidation occurs at 0.6 V and the metal oxide and oxygen reduction peak is seen at 0.7 V. Though the overall shape of the voltammograms is similar, there are several differences, which characterize the electrochemical behavior on the two surfaces. Firstly in the H_{upd} region, the platinum electrode exhibits 3 peaks, characteristic of the hydrogen adsorption on its different crystal faces. However, the palladium bimetallic catalyst, typical of a Pd electrode in acid solution, shows a single broad peak, which is due to the dissolution of the adsorbed hydrogen into the bulk of the Pd electrode [38,39]. Secondly, at moderate potentials corresponding to the double layer region, similarities in the magnitude of the double layer current verify similar electrode areas for the two electrocatalysts. Finally, in the oxide and oxygen reduction region at elevated potentials, the Pd catalysts show oxidation and reduction peaks at more negative potentials than Pt, again characteristic of Pd electrodes in acidic solutions. In this case, a shift of approximately 60 mV is observed between the $CoPd_3$ and Pt electrodes and the magnitudes of the peak currents are approximately equal. If the remaining terms from Eq. (10) are assumed constant, we may simplify Eq. (10) to emphasize the

rate constant dependence.

$$E_p = A + \frac{RT}{\alpha F} \ln (k_i) \tag{11}$$

We may also use Eq. (11) to compare the kinetic rate constants for the ORR on two different electrocatalysts by considering the difference in the reduction peak potentials.

$$E_{p2} - E_{p1} = \frac{RT}{\alpha F} \ln \left(\frac{k_2}{k_1} \right) \tag{12}$$

Inserting the values for the peak separation and assuming a transfer coefficient of 0.5 for the ORR on both electrodes, we find that the kinetic rate constant for the $CoPd_3$ electrode is approximately one-third that of polycrystalline platinum. This is consistent with recent work by Mustain [40] using an electrochemical interface model to describe ORR behavior on Pt, Pd and $CoPd_3$ rotating disk electrodes for the oxygen reduction in acidic solutions. Therefore, this small difference in the kinetic activity of the cobalt–palladium electrocatalyst is a significant result and further investigation into the kinetics and mechanism for the ORR on these electrocatalysts may provide an important insight into the synergistic role of secondary elements in bimetallic electrocatalysts for the ORR.

3.3. Kinetics and mechanism for the ORR on $CoPd_3$

Fig. 8 shows characteristic RDE voltammograms for the $CoPd_3$ electrode in oxygen saturated 0.5 M H_2SO_4 at 25 °C. The current densities were calculated by normalizing to the geometric electrode area. The potential regions under kinetic and oxygen mass transport limiting control are clearly observed for all of the rotation rates and the current density increases with increasing rotation rate as the mass transport of molecular oxygen to the electrode surface becomes facile. For quasi steady state conditions and assuming all of the reactions to be first order with respect to the reactant, the observed current, i, for a mixed kinetic-diffusion controlled reaction depends on the rotation rate

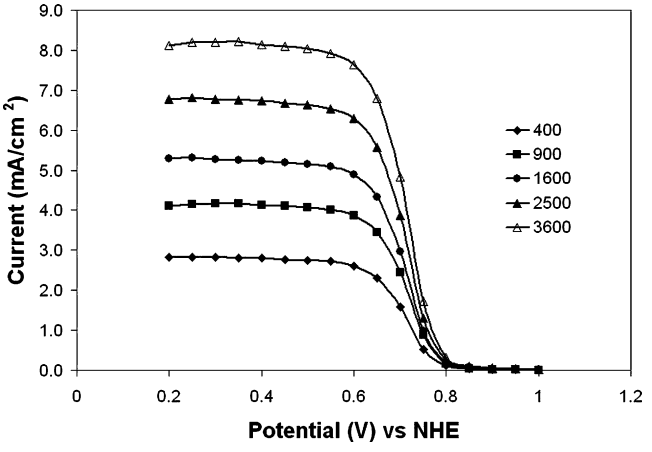

Fig. 8. Polarization experiments for a thin-film, polycrystalline $CoPd_3$ RDE at 25 °C in oxygen-saturated 0.5 M H_2SO_4 at 400 RPM (♦), 900 RPM (■), 1600 RPM (●), 2500 RPM (▲) and 3600 RPM (△), 10 mV s^{-1}.

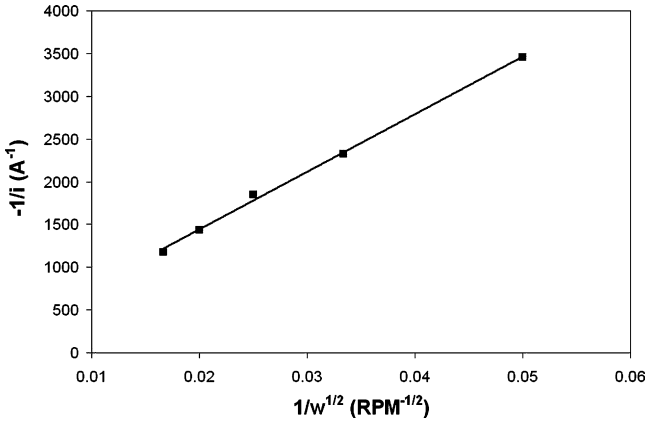

Fig. 9. Koutecky–Levich plot for the ORR on the $CoPd_3$ electrocatalyst RDE. n is calculated as approximately 4.0, indicating that the direct pathway is dominant.

according to the Koutecky–Levich equation [41].

$$\frac{1}{i} = \frac{1}{i_k} + \frac{1}{i_L} = \frac{1}{i_k} + \frac{1}{0.62nFAD^{2/3}C\nu^{-1/6}\omega^{1/2}} \tag{13}$$

where i_k is the kinetic current density for the ORR, i_L the mass transport limiting current, n the number of electrons involved in the ORR per oxygen molecule, C the saturation concentration for oxygen in water, D the aqueous binary diffusion coefficient, ν the kinematic viscosity of the solution and ω is the rotation rate. Fig. 9 presents the Koutecky–Levich plot, $1/i$ versus $1/\omega^{1/2}$, for $CoPd_3$ under mass transport control at an electrode potential of 0.2 V. Using the slope of the resulting linear relationship, the value for n was calculated to be 4.0, which is consistent with previous results by Adzic and coworkers [30] who calculated the value to be approximately 3.9 for a $CoPd_2$ electrocatalyst using a rotating ring-disk electrode (RRDE). This suggests that the ORR on $CoPd_3$ proceeds via the direct pathway involving the dual-site adsorbed oxygen species, given by Eq. (4) and illustrated in Fig. 2, since even highly active surfaces like Pt and its alloys that at least partially proceed via the peroxide route have n values slightly less than four [9,42]. Therefore, this result strongly suggests a high electrochemical efficiency for the $CoPd_3$ electrocatalyst, where virtually all of the O_2 is directly reduced to H_2O. However, due to experimental error and the limitations of the rotating disk electrode technique to fully describe the oxygen reduction reaction, verification of these results using the rotating ring-disk electrode technique to detect the peroxide intermediate desorption is critical and future work is aimed at doing this.

The first part of Eq. (13) can be rearranged in order to calculate the kinetic current for the ORR as a function of the potential.

$$i_k = \frac{i_L i}{i_L - i} \tag{14}$$

The overpotential equation for the kinetic current is given as Eq. (15).

$$\eta = a + b \log i \tag{15}$$

where η is the overpotential, a the Tafel intercept and b is the Tafel slope, which can be used to reveal properties of the rate-

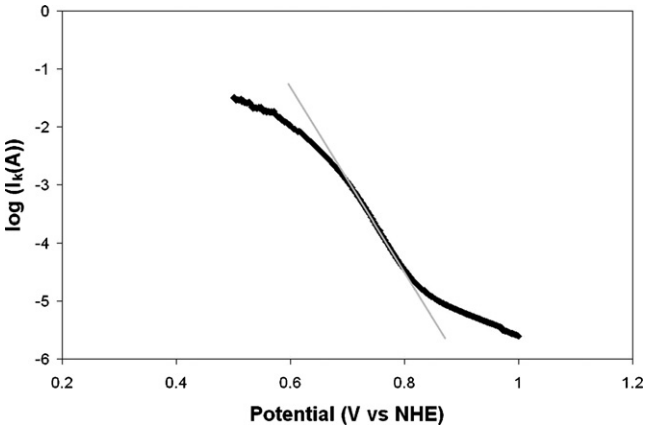

Fig. 10. Tafel plot for the $CoPd_3$ electrocatalyst at 25 °C, 2500 RPM. The Tafel slope was calculated as 70 mV decade^{-1}, indicating a chemical step following a fast first electron step is the rate-determining step.

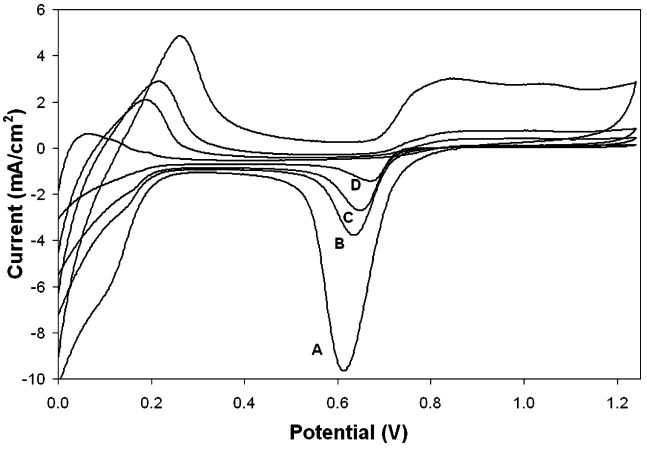

Fig. 11. Cyclic voltammograms of the electrodeposited $CoPd_3$ electrode in oxygen saturated 0.5 M H_2SO_4 at 22 °C, at scanrates of 0.5 V s^{-1} (A), 0.1 V s^{-1} (B), 0.05 V s^{-1} (C) and 0.01 V s^{-1} (D).

determining step. Fig. 10 shows a representative Tafel plot for ORR on $CoPd_3$ at 25 °C and 2500 RPM. Though two linear regions are observed in the Tafel plot for the ORR on $CoPd_3$, the low current density regime yields a slope of approximately 220 mV decade^{-1} for approximately one half order of magnitude of the kinetic current, which is suspect for both its value as well as its range. However, at more moderate current densities a clear linear region is observed between 0.8 and 0.65 V with a slope of 70 mV decade^{-1}. The 70 mV decade^{-1} Tafel is observed for approximately two and a half orders of magnitude of the kinetic current. The Tafel slope can then be used to calculate the effective transfer coefficient using Eq. (16).

$$b = \frac{RT}{\alpha n F} = \frac{60\,\text{mV decade}^{-1}}{\alpha} \tag{16}$$

where n is the number of electrons transferred, F the Faraday constant and α is the transfer coefficient, calculated as 0.86 for the ORR for $CoPd_3$.

A secondary method for calculating the transfer coefficient for an irreversible wave utilizes Eq. (10), which presents the peak potential, E_p, as a function of the scanrate. Bard and Faulkner [35] proposed that completely irreversible reactions show a negative shift for the peak potential of 30/α mV for each 10-fold increase in υ at 25 °C. Cyclic voltammograms for $CoPd_3$ in oxygen saturated 0.5 M H_2SO_4 at polarization scanrates of 0.01, 0.05, 0.1 and 0.5 volts per second (Vps) are presented in Fig. 11. The peak position is a clear function of the scanrate and the peak potentials are observed at 0.657 V for 0.01 Vps, 0.638 for 0.05 Vps, 0.631 for 0.1 Vps and 0.610 for 0.5 Vps. These results yield α values between 0.87 and 0.93 for the ORR, in reasonable agreement with the Tafel results.

Decomposition of the transfer coefficient can be used to determine nature of the rate limiting step in the ORR mechanism utilizing Eq. (17).

$$\alpha = \frac{\gamma}{\nu} + \rho\beta \tag{17}$$

where γ is the number of steps preceding the rate determining step, ν the stoichiometric coefficient, ρ equals 0 when the rate determining step is a chemical step and 1 if the rate determining step is an electron transfer step and β is the symmetric factor, which is 0.5 for most systems of interest [35]. If we estimate the transfer coefficient as 1.0 for the ORR on $CoPd_3$, the rate-determining step should be a chemical step following a fast first electron step. This is also supported by Fig. 12, which shows that the ORR on $CoPd_3$ is independent of the proton concentration, indicating that the rate determining step for the ORR cannot include a proton transfer or the desorption of a hydroxyl species.

If we consider a low Co-content cobalt–palladium bimetallic electrocatalyst where Co participates in the adsorption [26], the first electron transfer step in the ORR on $CoPd_3$ can be given as:

$$\text{Pd} + \text{Co} + \text{O}_2 + \text{e}^- + \text{H}^+ \rightarrow \text{PdOCoOH}_{\text{ads}} \tag{18}$$

Since the ORR on $CoPd_3$ proceeds through the direct mechanism, the first electron transfer is followed by the dissociation of the oxygen bond, which should be the rate determining step on the cobalt–palladium electrode as indicated by the calculated value for the transfer coefficient.

$$\text{PdOCoOH}_{\text{ads}} \rightarrow \text{PdO}_{\text{ads}} + \text{CoOH}_{\text{ads}} \tag{19}$$

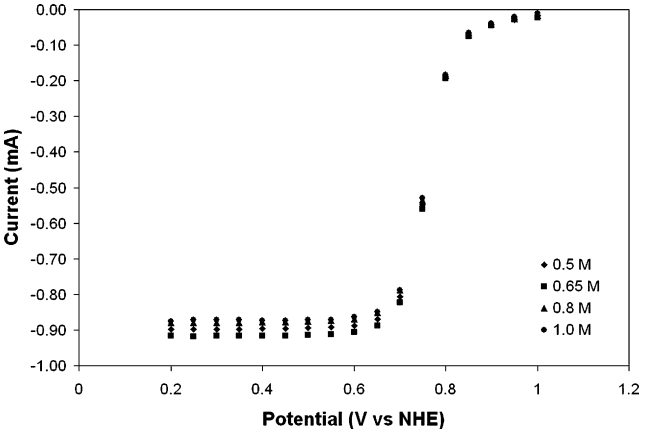

Fig. 12. RDE voltammogram for the prepared $CoPd_3$ electrode at 25 °C, 10 mV s^{-1}, 2500 RPM in oxygen saturated H_2SO_4 electrolyte of various compositions.

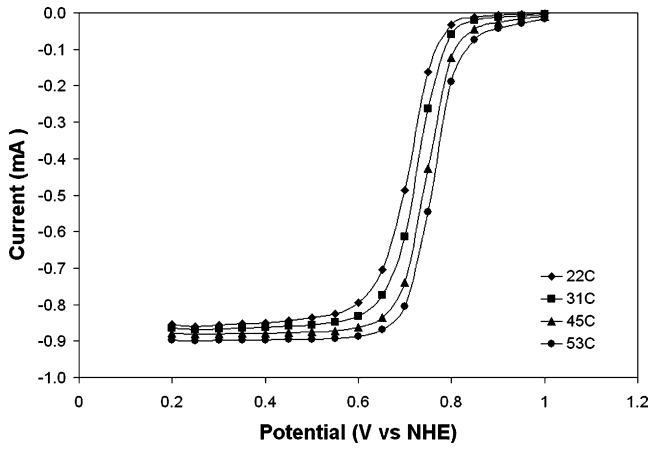

Fig. 13. RDE voltammogram for the $CoPd_3$ electrode at various temperatures between 22 and 53 °C, 10 mV s^{-1}, 2500 RPM in oxygen saturated 0.5 M H_2SO_4 electrolyte.

If the O–O bond breakage step is the rate determining step on $CoPd_3$, the magnitude of the activation energy should be similar to that of both Pt and Pd in acid media. RDE experiments were conducted various temperatures between 22 and 53 °C for the $CoPd_3$ electrocatalyst in oxygen saturated 0.5 M H_2SO_4 at 2500 RPM, presented as Fig. 13. A clear increase in the magnitude of the current in the kinetic regime was observed due to the overcoming of the activation barrier. Also, the mass transport controlled current is modestly increased due to slight increases in the diffusion coefficient at elevated temperatures. An Arhenius plot for the ORR at 0.8 V versus NHE on $CoPd_3$ is presented in Fig. 14 and the activation energy, E_a, was calculated according to the slope of the linear relationship.

$$\frac{\partial \ln(i)}{\partial(1/T)} = -\frac{E_a}{R} \tag{20}$$

where R is the ideal gas constant = 8.314 J mol^{-1} K^{-1}. The E_a was calculated as 49.5 kJ mol^{-1}, which is higher than recent values for Pt in acid media [43], though similar to early experimental values reported by Appleby in H_3PO_4 electrolyte [44]. The activation energy on Pt and Pd has been commonly attributed to the breaking of the oxygen bond [45–47]. Therefore, the Arhenius data seems to support the Tafel results that the O_2 bond breakage step is the rate determining step for $CoPd_3$.

This analysis has shown that a site mechanism is active for the oxygen reduction on cobalt–palladium electrocatalysts, where $CoPd_3$ is the electrochemically active site. Also, the ORR proceeds almost entirely through the complete four electron reduction, possibly through the bridge configuration involving both cobalt and palladium atoms. This is supported by Krawczyk and Sobczak [48] who discussed the dissociative adsorption of O_2 on cobalt–palladium alloys and found that the oxygen adsorption was promoted by an increase in the cobalt surface concentration. It was also shown that the rate determining step for the oxygen reduction on $CoPd_3$ is a chemical step, with no pH dependence, following a fast first electron transfer step, which is most likely the breaking of the oxygen bond. Also, previous theoretical work by Mustain [40] indicated that the Co atom was the electron transfer site. Therefore, the proposed reaction mechanism and adsorption behavior for molecular oxygen on $CoPd_3$ is illustrated in Fig. 15, where cobalt atoms are indicated by gray, outlined circles and adsorbed oxygen atoms are indicated by smaller, completely darkened circles.

Though the atomic mechanism proposed in Fig. 15 is consistent with the experimental data for a single oxygen molecule, it is clear that this simple mechanism does not fully describe the oxygen reduction on cobalt–palladium electrocatalysts. First, the atomic mechanism does not explain why $CoPd_3$ is the optimum electrocatalytic site for the oxygen reduction reaction as a single oxygen molecule is shown interacting with one cobalt and one palladium atom. Also, following the oxygen bond breakage step, the cobalt atom is left with an adsorbed hydroxyl species, Co–OH. This indicates that the Co atom should have a +1 oxidation state, which not a valid oxidation state for cobalt. However, since Cobalt has been identified as the electron transfer site for the oxygen reduction reaction, Co–OH is a necessary intermediate following the electron transfer step.

Therefore, owing to the stable cobalt oxidation states, Co(II) and Co(III), it is possible that the cobalt atom may participate in the adsorption and electron transfer of more than one oxygen molecule, forming either Co–$(OH)_2$ or Co–$(OH)_3$. Both species

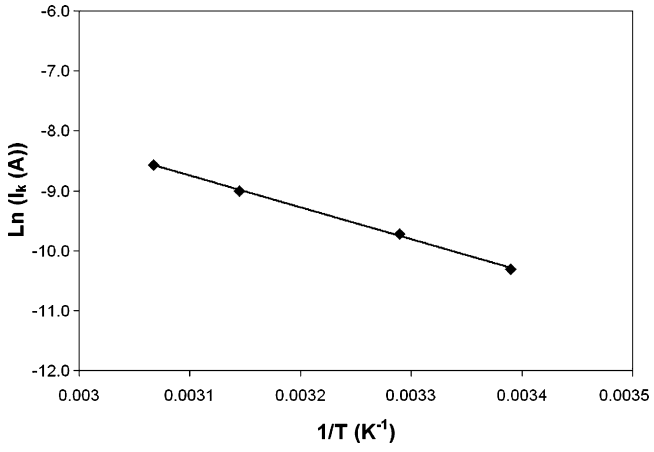

Fig. 14. Arhenius plot for the ORR on $CoPd_3$. The activation energy is calculated from the slope = $-E_a/R$.

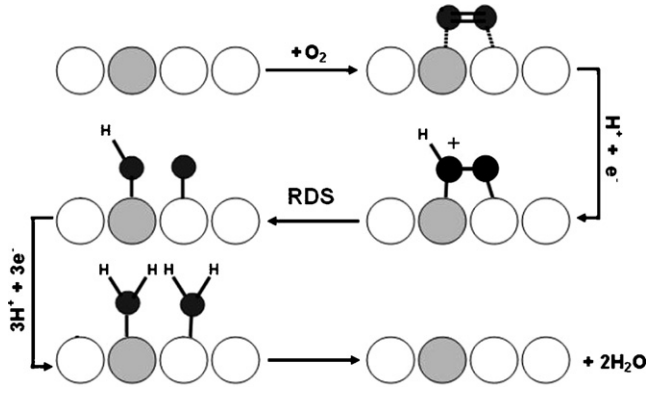

Fig. 15. Proposed atomic-scale mechanism for the oxygen reduction reaction on cobalt–palladium electrocatalysts in acid media. The unfilled circles represent Pd, grayed circles represent Co and small black circles represent oxygen.

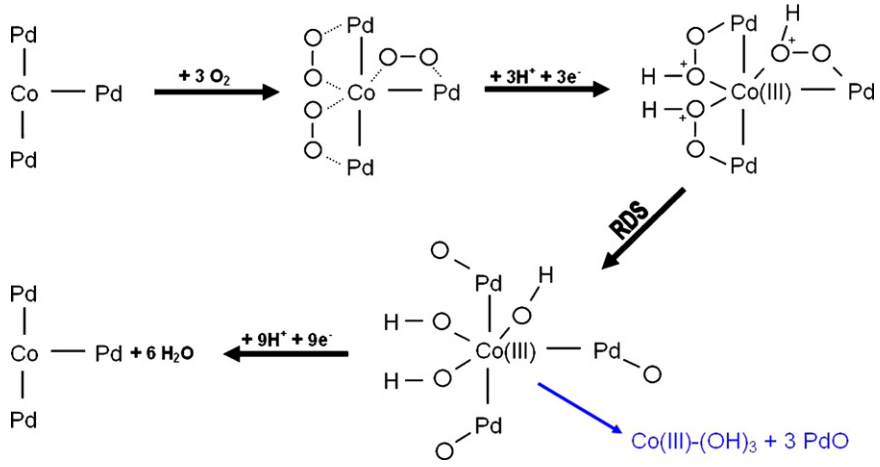

Fig. 16. $CoPd_3$ active site mechanism for the oxygen reduction reaction on cobalt–palladium electrocatalysts in acid media.

are well known, stable cobalt complexes in acid solutions. However, evidenced by the magnitude of the Gibbs free energy for the electrochemical reductions as well as the identification of $CoPd_3$ as the electrochemically active site, Co–$(OH)_3$ is the likely reaction intermediate, where the one electron transfer step for the oxygen reduction is performed three times at each cobalt atom. This is also validated in light of a study by Armstrong et al. [49], where it was shown that Co(III) incorporated into a nickel hydroxide matrix affected the oxygen reduction kinetics.

The expanded mechanism, incorporating the electrochemically active $CoPd_3$ site for the ORR, is illustrated in Fig. 16. The suggested mechanism clearly displays the critical features of the oxygen reduction reaction, including the bridge-bonded adsorption leading to the complete four electron reduction, the first electron transfer step forming Co–(OH) species, and the oxygen bond breakage step, which has been electrochemically identified as the rate determining step on the $CoPd_3$ electrocatalyst. The mechanism presented in Fig. 16 also proposes a truly synergistic mechanism for the ORR on cobalt–palladium bimetallic electrocatalysts; however, further physical and electrochemical characterization is necessary in order to validate the proposed mechanism and future work is aimed at doing this.

4. Conclusions

Polycrystalline cobalt–palladium electrocatalysts of various compositions were prepared and both their physical properties and electrochemical activity for the ORR were examined. The prepared $CoPd_x$ electrocatalysts were single phase, homogeneous and displayed the face centered cubic structure. Voltammetric analysis revealed that the $CoPd_x$ electrodes showed substantial activity for the ORR, where $CoPd_3$ was the best. RDE analysis revealed that the ORR on $CoPd_3$ proceeds via the direct route leading to the complete four-electron reduction to water. It was shown that the rate determining step on $CoPd_3$ is a chemical step that follows the fast first electron transfer step and it is proposed that this step includes the breaking of the O–O bond. Also, specific ways that the surface structures are involved was proposed, explaining why $CoPd_3$ shows the best activity for the ORR.

Acknowledgements

This work was supported by the Brookhaven National Laboratory through a subcontract under the U.S. Department of Energy, Divisions of Chemical and Material Sciences, contract no. DE-AC02-98CH1-886. The authors would like to thank Dr. R. Adzic of Brookhaven National Laboratory for useful discussions.

References

[1] K. Kinoshita, Electrochemical Oxygen Technology, Wiley, USA, New York, 1992.
[2] T.E. Springer, M.S. Wilson, S. Gottesfield, J. Electrochem. Soc. 140 (1993) 3513.
[3] R. Mosdale, S. Srinivasan, Electrochim. Acta 40 (1995) 413.
[4] J.S. Newman, Electrochemical Systems, Prentice Hall, 1991.
[5] V. Stamenkovic, T.J. Schmidt, P.N. Ross, N.M. Markovic, J. Phys. Chem. B 106 (2002) 11970.
[6] A.B. Anderson, J. Roques, S. Mukerjee, V.S. Murthi, N.M. Markovic, V. Stamenkovic, J. Phys. Chem. B 109 (2005) 1198.
[7] S. Mukerjee, S. Srinivasan, M.P. Soriaga, J. BcBreen, J. Electrochem. Soc. 142 (1995) 1409.
[8] S. Mukerjee, S. Srinivasan, J. Electroanal. Chem. 357 (1993) 201.
[9] U.A. Paulus, A. Wokaun, G.G. Scherer, T.J. Schmidt, V. Stamenkovic, V. Radmilovic, N.M. Markovic, P.N. Ross, J. Phys. Chem. B 106 (2002) 4181.
[10] N.M. Markovic, C. Lucas, V. Climent, V. Stamenkovic, P.N. Ross, Surf. Sci. 465 (2000) 103.
[11] V. Climent, N.M. Markovic, P.N. Ross, J. Phys. Chem. B 104 (2000) 3116.
[12] C.A. Lucas, N.M. Markovic, P.N. Ross, Phys. Rev. B 55 (1997) 3368.
[13] B. Beard, P.N. Ross, J. Electrochem. Soc. 137 (1990) 3368.
[14] J.T. Glass, G.L. Cahen, G.E. Stoner, J. Electrochem. Soc. 134 (1987) 58.
[15] U.A. Paulus, G.G. Scherer, A. Wokaun, T.J. Schmidt, V. Stamenkovic, V. Radmilovic, N.M. Markovic, P.N. Ross, J. Phys. B 106 (2001) 4181.
[16] T. Toda, H. Igarashi, H. Uchida, M. Watanabe, J. Electrochem. Soc. 141 (1999) 968.
[17] T. Toda, H. Igarashi, H. Uchida, M. Watanabe, J. Electrochem. Soc. 146 (1999) 3750.
[18] N.M. Markovic, P.N. Ross, in: Wieckowski (Ed.), Interfacial Electrochemistry. Theory, Experiment and Applications, Marcel Dekker, New York, 1999, p. 821.
[19] P.B. Balbuena, D. Altomare, L.A. Agapita, J.M. Seminario, J. Phys. Chem. B 107 (2003) 13671.
[20] J.M. Seminario, L.A. Agapito, L. Yan, P.B. Balbuena, Chem. Phys. Lett. 410 (2005) 275.

[21] A. Damjonovic, V. Brusic, Electrochim. Acta 12 (1967) 625.
[22] E.B. Yeager, Electrochim. Acta 29 (1984) 1527.
[23] Y. Wang, P.B. Balbuena, J. Phys. Chem. B 108 (2004) 4376.
[24] R.A. Sidik, A.B. Anderson, J. Electroanal. Chem. 528 (2002) 69.
[25] J. Zhang, M.B. Vukmirovic, Y. Xu, M. Mavrikakis, R.R. Adzic, Angew. Chem. Int. Ed. 44 (2005) 2132.
[26] J.L. Fernandez, D.A. Walsh, A.J. Bard, J. Am. Chem. Soc. 127 (2005) 357.
[27] W.E. Mustain, K. Kepler, J. Prakash, Electrochem. Commun. 8 (2006) 406.
[28] V. Raghuveer, A. Manthiram, A.J. Bard, J. Phys. Chem. B 109 (2005) 22909.
[29] O. Savadogo, K. Lee, K. Oishi, S. Mitsushima, N. Kamiya, K.I. Ota, Electrochem. Commun. 6 (2004) 105.
[30] M.H. Shao, T. Huang, P. Liu, J. Zhang, K. Sasaki, M.B. Vukmirovic, R.R. Adzic, Langmuir 22 (2006) 10409.
[31] S.N. Vinogradov, Prot. Met. (Russian: Zaschita Mettalov) 14 (1978) 362.
[32] E.V. Chumak, Russ. J. Electrochem. (Russian: Elektrokhimiya) 25 (1989) 1668.
[33] J.A. Abys, I. Boguslavsky, J.K. Straschil, US Patent No. 5,976,344 (1999).
[34] A. Miyazaki, I. Balint, Y. Nakano, J. Nanoparticle Res. 5 (2003) 69.
[35] A.J. Bard, L.R. Faulkner, Electrochemical Methods, Wiley, New York, 2001.
[36] J.F. Drillet, A. Ee, J. Friedemann, R. Kotz, B. Schnyder, V.M. Schmidt, Electrochim. Acta 47 (2002) 1983.
[37] H.A. Gasteiger, W. Gu, R. Makharia, M.F. Mathias, B. Sompalli, in: W. Vielstich, A. Lamn, H. Gasteiger (Eds.), Handbook of Fuel Cells, vol. e, Wiley, New York, 2003.
[38] A.J. Bard, Electroanalytical Chemistry, vol. 9, Marcel Dekker, Inc., New York, 1976, p. 109.
[39] M. Enyo, T. Yamazaki, K. Kai, K. Suzuki, Electrochem. Acta 28 (1983) 1573.
[40] William Mustain, PhD Thesis, Illinois Institute of Technology, 2006.
[41] V.G. Levich, Physicochemical Hydrodynamics, Prentice Hall, 1962.
[42] T. Ioroi, K. Yasuda, J. Electrochem. Soc. 152 (2005) A1917.
[43] A.B. Anderson, T.V. Albu, J. Electrochem. Soc. 147 (2000) 4229.
[44] A.J. Appleby, in: B.E. Conway, J.O. Bockris, E. Yeager, S.U.M. Khan, R.E. White (Eds.), Comprehensive Treatise of Electrochemistry, vol. 7, Plenum Press, New York, 1983 (Chapter 4).
[45] R. Adzic, in: J. Lipkowski, P.N. Ross (Eds.), Electrocatalysis, Wiley–VCH, New York, 1998.
[46] D.B. Sepa, M.V. Vojnovic, A. Damjanovic, Electrochim. Acta 25 (1980) 1491.
[47] E. Yeager, J. Mol. Catal. 28 (1986) 5.
[48] M. Krawczyk, J.W. Sobczak, Appl. Surf. Sci. 235 (2004) 49.
[49] E.D. Armstrong, G.W.D. Briggs, E.A. Chambers, J. Appl. Electrochem. 18 (1988) 215.